Using Ansys for Design and Numerical Study of a Specific Fixed Wing UAV

GABRIEL MURARIU[1]*, RAZVAN ADRIAN MAHU[2], ADRIAN GABRIEL MURARIU[3], MIHAI DANIEL DRAGU[1], LUCIAN P. GEORGESCU[1], BOGDAN G. CARP[2]

[1] Dunarea de Jos University of Galati, Chemistry, Sciences and Environment Faculty, Physics and Environment Department, Romania, 47 Domneasca Str., 800080, Galati, Romania

[2] Dunarea de Jos University of Galati, Faculty of Engineering, 47 Domneasca Str., 800080 Galati, Romania

[3] Department of Physics, Imperial College London, Kensington, London SW7 2AZ, UK

This article presents the design of a specific unmanned aerial vehicle UAV prototype own building. Our UAV is a flying wing type and is able to take off with a little boost. This system happily combines some major advantages taken from planes namely the ability to fly horizontal, at a constant altitude and of course, the great advantage of a long flight-time. The aerodynamic models presented in this paper are optimized to improve the operational performance of this aerial vehicle, especially in terms of stability and the possibility of a long gliding flight-time. Both aspects are very important for the increasing of the goals' efficiency and for the getting work jobs. The presented simulations were obtained using ANSYS 13 installed on our university' cluster system. In a next step the numerical results will be compared with those during experimental flights. This paper presents the main results obtained from numerical simulations and the obtained magnitudes of the main flight coefficients.

Keywords: numerical simulations, flight coefficients, flying wing

Currently, the emphasis on economic grounds for reducing the costs led to the idea of developing for unmanned aircraft [1, 2]. Unmanned aerial vehicles (UAV) are usually multi-purpose devices. This is by the fact that UAV are very compact and mainly because are ease of use. This led to the award of various missions because they have won a number of outstanding capabilities in recent decades [2]. These aerial robots can be used in a variety of civilian missions such as disaster monitoring, traffic monitoring, enforcement and power line maintenance [2].

UAVs are important primarily because of their ability to replace manned aircraft in routine tasks or especially in dangerous missions' cases. A second argument comes from the fact that unmanned aerial vehicles can reduce the cost of air operations [2]. For example, the presented system has a level of cost for an hour of flight time over a liter of gasoline.

In principle, a UAV system consists of two parts: an active element (the vehicle itself) and the second - a ground-station for control and video receiving. The UAV control can be achieved either by using a manual piloting unit or by using the flight controls in auto-pilot mode, by integrating a GPS system for flight routes.

Due to their low-risk, low-cost, high turn-over of operation these devices present certain benefits and advantages that are unrivaled.

As the main advantages of UAVs, we can list: a) could be used in high risk situations and inaccessible areas; could offer possibilities of data acquisition with high temporal and spatial resolution; c) low-cost of operation (a fraction of the cost of operation of a traditional plane with human pilot onboard).

Unfortunately, there are a series of limitations in the use of UAV's which could hang tough in choosing a suitable means: a) the main disadvantage in due by the limitations of the payload; b) the UAV hove to use of low-weight sensors (this becomes less and less important during the time since the technology advances).

These application domains have led to the development of more advanced research to increase the autonomy and reducing the UAVs size basing on a performing design. In this order, the dynamical performance of machinery can be improved dramatically in certain cases through a systematic and meticulous evolutionary algorithm search through the space of all structural geometries permitted by manufacturing, cost and functional constraints [3].

These flying robots called UAV can be classified into three main categories: 1) fixed-wing UAVs, 2) rotary wing UAVs, 3) hybrid design UAVs.

Fixed-wing UAVs are the richest group among these three categories, both in terms of research and use. These devices are capable of long flight-time gliding at a enough speeds low speed in order to be able to make a proper supervision. Their design is simple, in comparison with other types of UAVs. The advantages of these types of UAVs are balanced by a number of disadvantages such as the inability to fly to a respective fixed point and the inability to scan an area with very low speed, the speed is limited by the necessity of a minimal lift force existence.

Given the disadvantages, in many cases, fixed wing UAVs require runways or additional launch and recovery equipment, used for takeoff and landing. For rotary wing UAVs and for the hybrids UAVs can be enumerated a number of complementary advantages with respect to the first UAVs category: flight at a fixed point, the possibility of investigating low speed zones, etc. For comparison, rotary wings UAVs are advantageous from this point of view, since they do not require any infrastructure for takeoff and landing.

The presented paper present preliminary results of constructing efforts for a specific fixed-wing UAV type device with smaller dimensions for an adequate payload. In the future work, will be presented a specific application [5].

The geometry

Given the current practice from the need of a wing with greater stability in flight, the flying wing concept is most practical for small gear models.

* email: *gabriel.murariu@ugal.ro*

A flying wing is sometimes presented as, at least in theory, the most efficient configuration in terms of aerodynamics. Also, this structure would provide the highest structural efficiency for depth on the wing, which results in a lightweight and ultra-light wing loading and hence high efficiency in terms of fuel consumption. The efficiency is based on the used airfoil profile.

In a previous work were exposed the reasons and results of the analysis after which, we opted for a NACA profile [3].

Due to favorable aerodynamic properties, especially due to torque coefficient' magnitude which is close to zero, a very similar profile with the NACA flying wing was selected in order to build the presented model. The above coefficient is very important for the aerodynamic feature for this UAV.

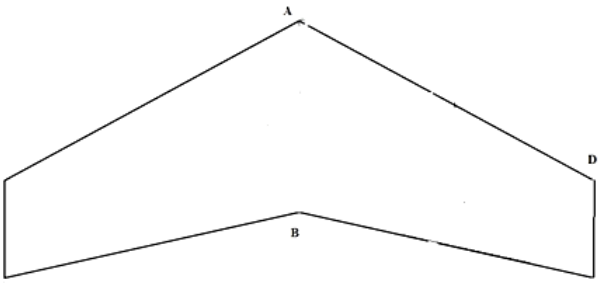

Fig. 1. The chosen geometry for the flying wing configuration

Our proposed design should be simpler compared to other types of fixed-wing UAVs and thus, in the case of our own prototype, was selected the wing structure type and geometry used is shown in figure 1. This configuration is chosen as the starting point of the study will be presented below.

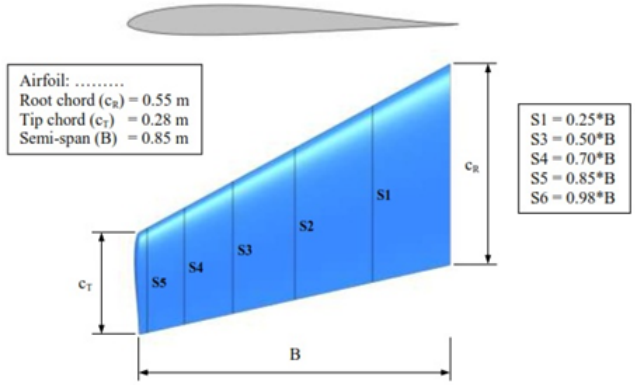

Fig. 2 - The geometry of plane wing and the reference profile used in numerical modeling and the sections for which have been calculated the pressure coefficient profiles (S1 - S5)

Due to idea to facilitate the execution, the dihedral angle of the wing was imposed null. Also it was not applied tension in the scope.

The first stage was to realize a numerical simulation in order to succeed in spotting the main flight coefficients and the preliminary results are the subject of this paper.

For the numerical grid construction, by the condition that the shape of the base and the edge profile has to be the same, the wing area results by a simple linear interpolation.

In order to come the numerical model' geometry closer to reality, the shape of the reference profile was modified by thickening its trailing edge by up to 2 mm (0.0036cb or 0.0072 cT).

Even though, the numerical model was achieved by rounding subsequently to improve the dynamic behavior and performance. For this, it was decided a fitment of winglets.

Numerical modeling

For the computational domain (fig. 3) it was chosen as a semi-spherical shape, taking into account the symmetry of the wing. Assuming this symmetry, the flow was simulated only for the left half-plane flying wing, which reduced the computational effort at half. Diameter calculation domain was chosen equal to

$$D = 25\,(c_R + c_{RT}) / 2 \qquad (1)$$

i.e about 25 times the mean aerodynamic chord [4].

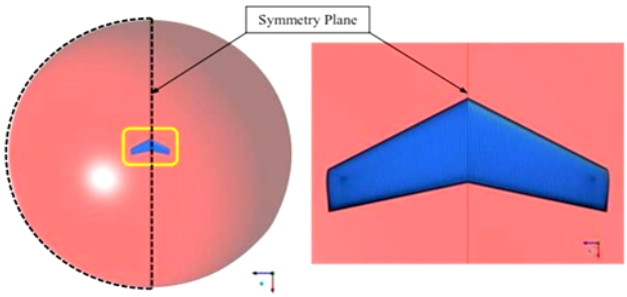

Fig. 3. The computing field, the used symmetry plane and the wing surface mesh

In the following section, it will be presented the main steps for the numerical approach. For the discretisation, it was choose a multi-block structured method which is the most suitable procedure for the geometries of this type. At the same time, the degree of precision that could be achieved with mesh of this type can be superior unstructured mesh type. From figure 4 we can see the density and distribution of grid nodes and also special smoothness of the grid, obtained by applying elliptic algorithms. More attention was given to the area near the wall of the wing, where the presence of the boundary layer requires a very fine meshing (the height of the first layer of cells was chosen so that the parameter y + is approximately equal to 1). The result is a grid mesh of very good quality, with an estimated 7.5 million finite volumes.

The fluid flow modeling (air at standard conditions of pressure and temperature) was obtained using an incompressible Navier-Stokes model (due to reduced velocities). For the turbulence modeling was considered the Shear-Stress Transport k-omega model [4, 5]. The grid density in the boundary layer allows avoiding the use of wall functions.

Boundary condition applied to the outer surface of the computing field has been set to be VELOCITY-INLET. The outer surface is hemispherical. The velocity vector direction is specified so that it can get different angles of attack (AOA).

Flow simulation was performed using ANSYS Fluent software v13.0 and the simulations were run on our university kernel.

Using a coupled implicit solver type, the numeric convergence solution was obtained in 300-500 iterations. To monitor convergence were applied equations' residues both for coefficients and aerodynamic forces [6, 7].

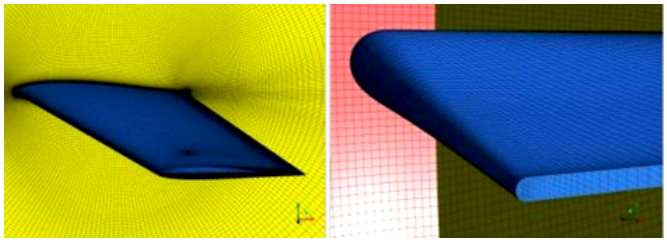

Fig. 4.Details of the mesh: the symmetry plane (left) and wingtip (right)

Results and discussions

Figures 5.a-5.f show the flying wing aerodynamic performance. The calculated values are relative to the reference area A_{ref} = 0.7055 [m²] and the speed of evolution V_{ref} = 50 [km/h] which is a necessary speed for the research procedures [3].

The aerodynamic stall phenomenon' occurrence, limits the useful incidence to more than 13 degrees. Actually, it is happened not because the lift effect' stagnation, but due to a sharp increase of the resistance force (basically, the CD is doubled from 13 to 15 deg AOA).

Maximum value for the lift coefficient (C_L = 0.9) is obtained at a value of AOA = 13 deg. (fig. 5.a). These relatively right values are obtained due to the considered profile and are in a good concordance with the NACA databases simulations (http://www.ppart.de / aerodynamics /profiles /NACA4.html).

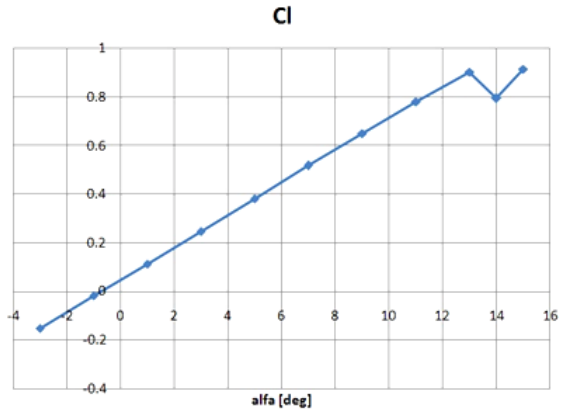

Fig. 5.a. The lift coefficient C_L for different values of AOA for a velocity of 50 km/h

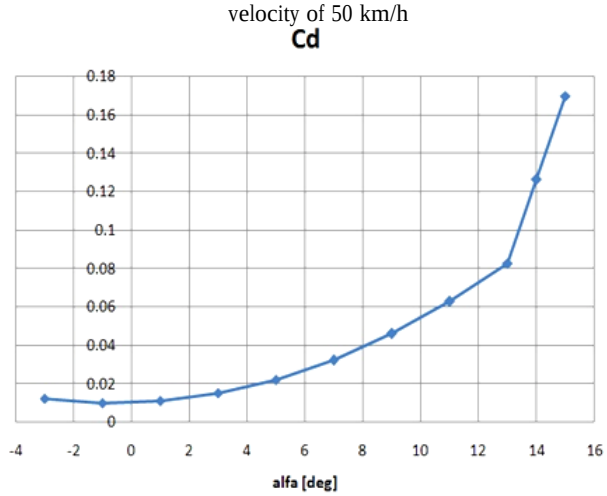

Fig. 5.b. The drag coefficient C_d for different values of AOA for a velocity of 50 km/h

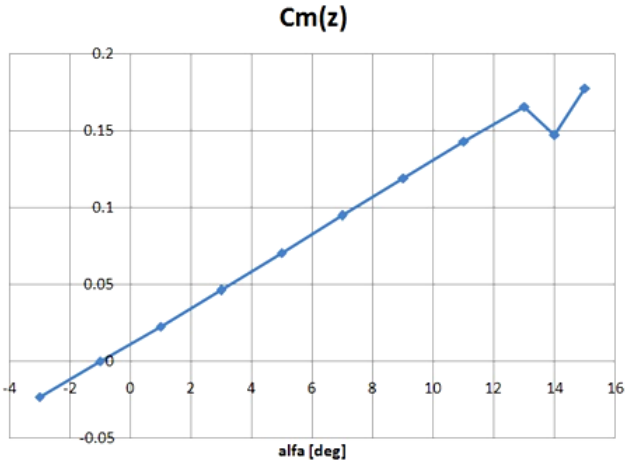

Fig. 5.c. The momentum coefficient C_m for different values of AOA for a velocity of 50 km/h

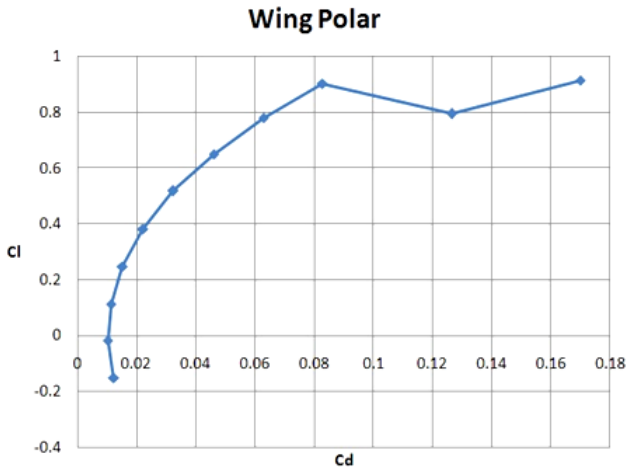

Fig. 5.d.The wing polar characteristics for different values of AOA for a velocity of 50 km/h

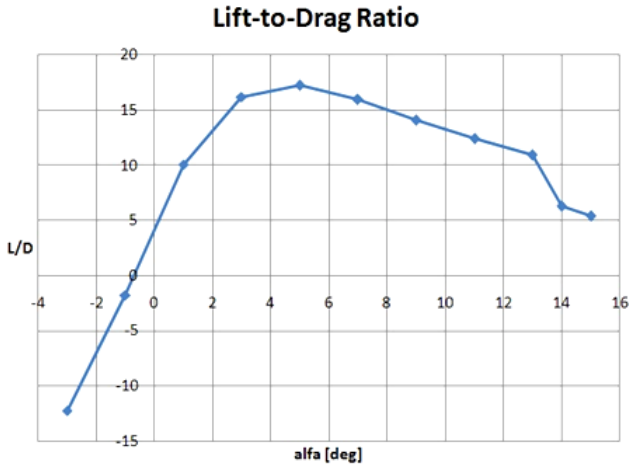

Fig. 5.e.The lift to drag characteristics for different values of AOA for a velocity of 50 km/h

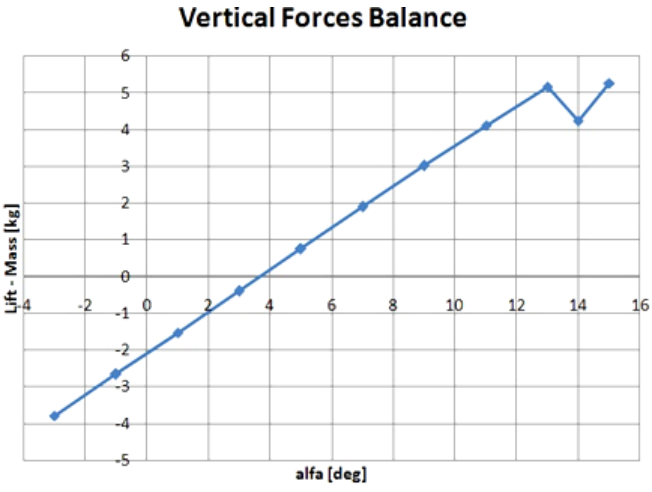

Fig. 5.f.The vertical force characteristics for different AOA values for a velocity of 50 km/h

The minimum value for the drag coefficient (C_d = 0.01) is reached at AOA = -1 deg (fig. 5b) which is an advantage. The momentum coefficient has same characteristic as the lift coefficient therefore the pressure center has a good stability.

The ratio of lift force and the drag dependency of AOA (fig. 5.d) are very interesting. Between 1 degree and 13 AOA, the ratio C_L/C_D is greater than 10. Between 2.5 and 8 degrees AOA is over 15 and the optimum C_L/C_D = 17 (highly favorable value) is around 5 degrees AOA. This indicates a high degree of flexibility configuration in studied

aerodynamics application and further in the research purpose.

Balance of forces in the vertical direction representation (fig. 5.f) indicates the possibility of flying wing load evaluation. Thus, for a speed of 50 km/h, and the optimum incidence angle AOA = 5 degrees, maximum loading capacity is about of 0.8 kg which is enough for our research purpose [3].

The aerodynamic stall phenomenon' occurrence, limits the useful incidence to more than 13 degrees. Actually, it is happened not because the lift effect' stagnation, but due to a sharp increase of the resistance force (basically, the C_d is doubled from 13 to 15 degrees AOA).

In figures 6.a - 6.d are represented the static pressure distribution on the wing extrados at different angles of incidence. These pictures highlight the mechanism which leads to airflow separation and rapid changes in the aerodynamic characteristics of the wing as it was shown in figures 5.

As could be seen in figure 6.a, for an AOA of 11 degrees, in the absence of torsion in scope, local aerodynamic incidence is approximately constant along the length of the wing leading edge. For this AOA the air flow has a nice pressure distribution along the wing.

Due to the fact that the wing is generated by scaling the base profile, the curvature of the leading edge to the peak increases. In the same time the adverse pressure gradient on the upper side increases too (fig. 6.b) [2, 5-7]. Consequently, somewhere between 13 and 14 degrees, the phenomenon of aerodynamic stall appears which means the air fillets separation and an alteration of the pressure distribution (fig. 6.c - fig. 6.d).

With the increasing AOA, the detachment extends to the wing. To delay this phenomenon, it could be considered a torsion wing with the decrease of the incidence angle geometry from base to tip of the wing.

Figures 7.a - 7.d present the pressure coefficient distributions calculated in the five sections (S1-S5) for different angles of attack. On the X-axis is represented the dimensionless position obtained by referencing to the value of the wing chord profile in the base section (CR), originating in its leading edge (fig. 2).

One can easily see how, as long as the flow remains attached to the wing, the loading increases from bottom to approximation in the right section S3 (0.70 B) and further decreases the top (fig. 7.b, fig. 7.c and fig. 7.d).

The pressure profile shape coefficient at S5 position indicates local effects due to fluid circulation around the end of the wing. This phenomenon is limited by the introduction of winglets sites.

From the figures 7.c and figure 7.d could be seen that the separation flow is evident in the incidence angles above 13 degrees' case.

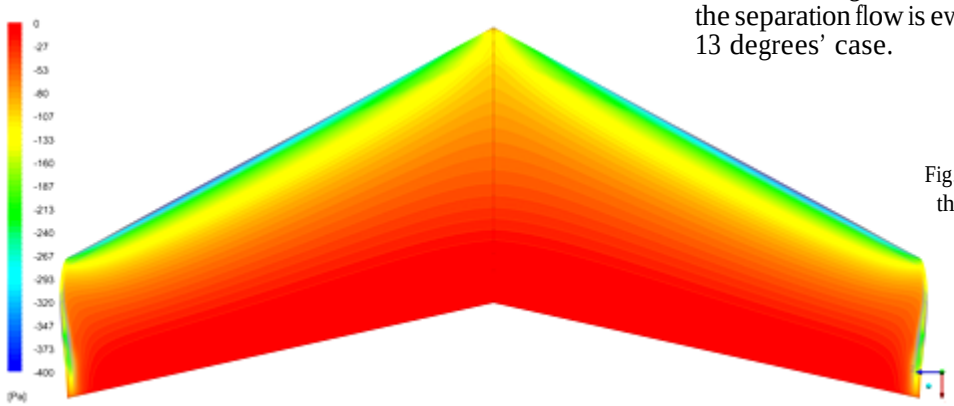

Fig. 6.a. The static pressure distribution on the wing extrados for an AOA value of 11 degrees for a velocity of 50 km/h

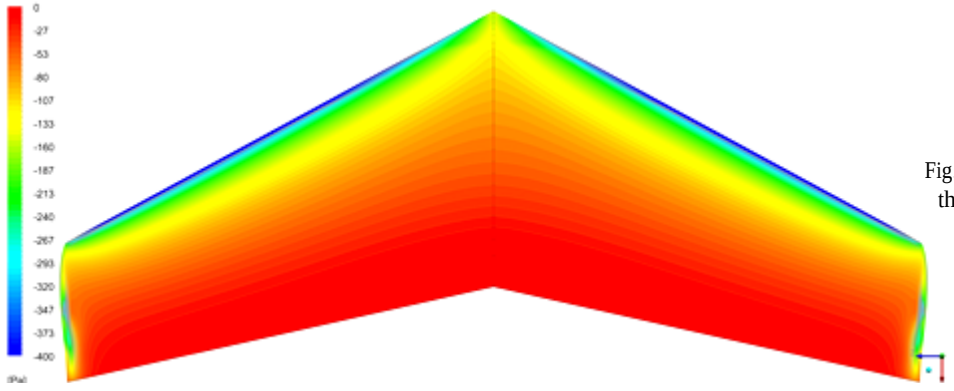

Fig. 6.b. The static pressure distribution on the wing extrados for an AOA value of 12 degrees for a velocity of 50 km/h

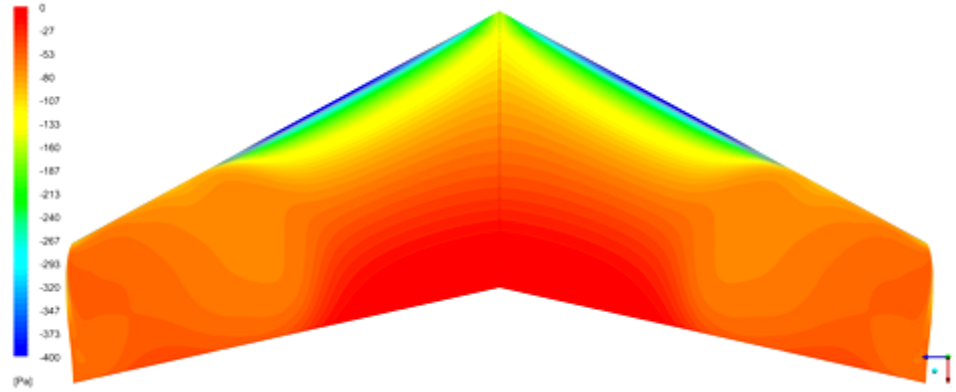

Fig. 6.c. The static pressure distribution on the wing extrados for an AOA value of 13 degrees for a velocity of 50 km/h

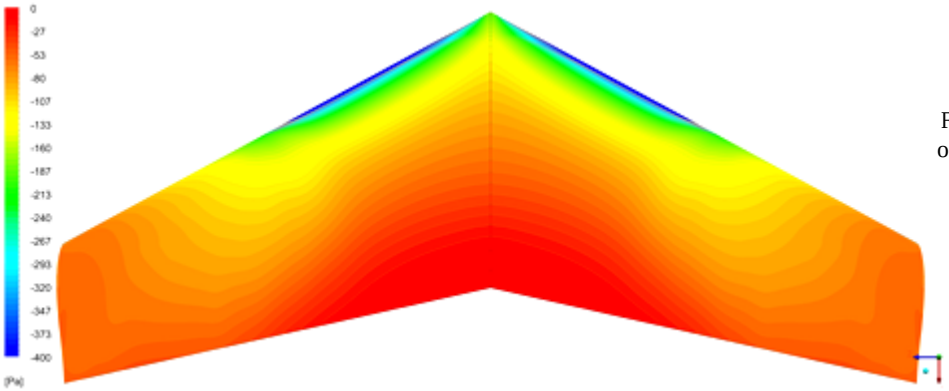

Fig. 6.d- The static pressure distribution on the wing extrados for an AOA value of 14 degrees for a velocity of 50 km/h

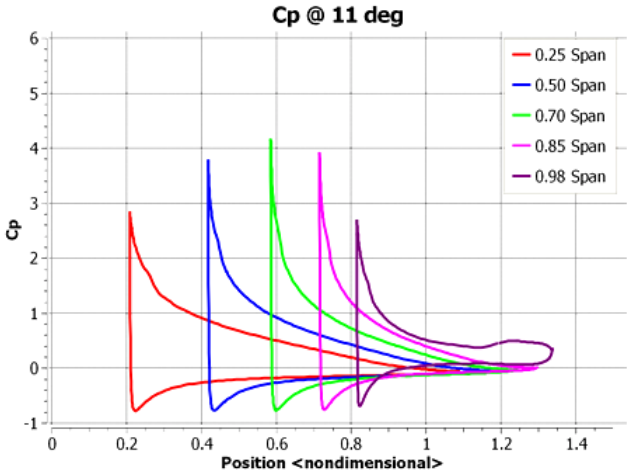

Fig. 7.a- The pressure coefficient distributions calculated in the five sections (S1-S5) for an AOA value of 11 degrees for a velocity of 50 km/h

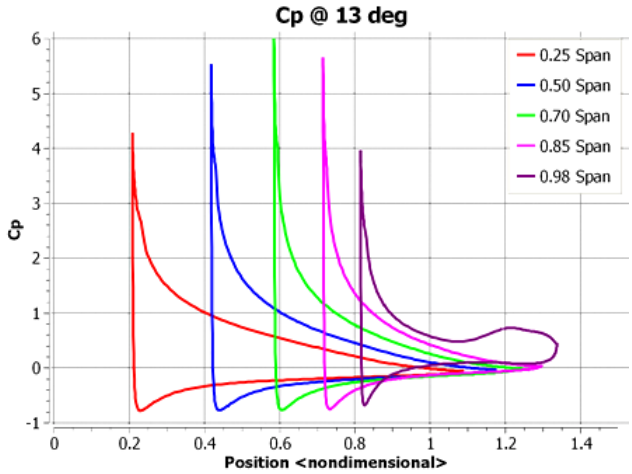

Fig. 7.b- The pressure coefficient distributions calculated in the five sections (S1-S5) for an AOA value of 13 degrees for a velocity of 50 km/h

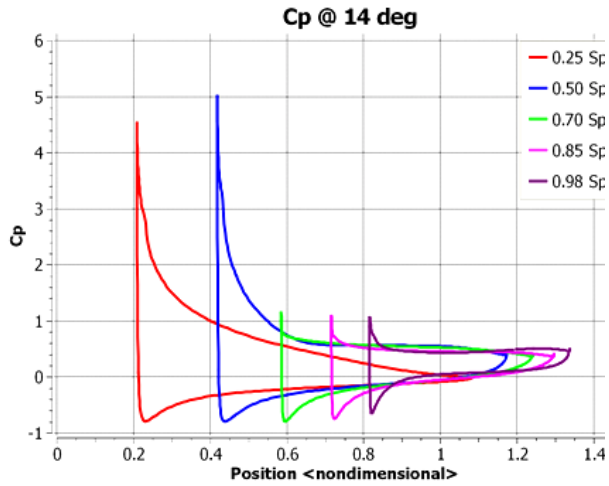

Fig. 7.c- The pressure coefficient distributions calculated in the five sections (S1-S5) for an AOA value of 14 degrees for a velocity of 50 km/h

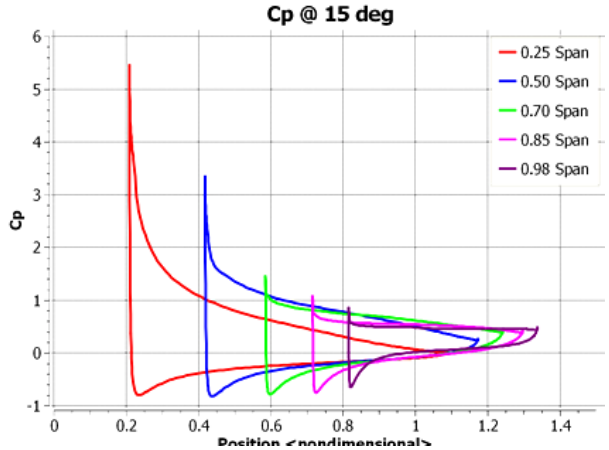

Fig. 7.d- The pressure coefficient distributions calculated in the five sections (S1-S5) for an AOA value of 15 degrees for a velocity of 50 km/h

Movement of the fluid flow near the extrados of the wing area is outlined in figure 8a.-8.d. The representation is made by the overlap of power lines and the local coefficient of friction at the wall.

One can immediately see the effect of adverse pressure gradient from the trailing edge, respectively the deflection of the power lines outward. This effect is more obvious with the increasing of the angle of incidence (fig. 8, b).

The aerodynamic stall phenomenon appearance drastically changes the power lines' spectrum in the area affected by the separation (ig. 8c, fig. 8.d).

In this area, the flow reversal is local. Although friction forces change their meaning portion detachment, this cannot compensate for the unfavorable distribution of static pressure, lowering the aerodynamic performances.

Figure 9 details the phenomenon of detachment, being able to easily identify the recirculation zone that starts from the leading edge of the wing, dominated by low speed and reverse flow.

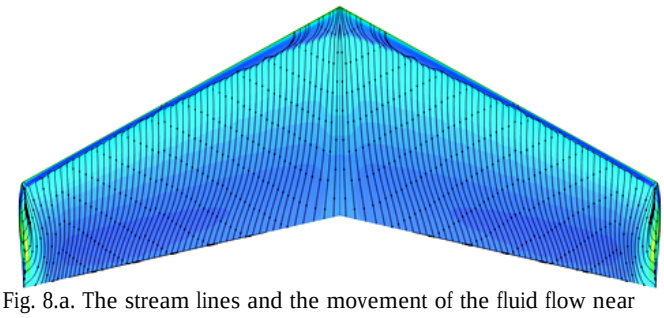

Fig. 8.a. The stream lines and the movement of the fluid flow near the extrados for an AOA value of 11 deg. for a velocity of 50 km/h

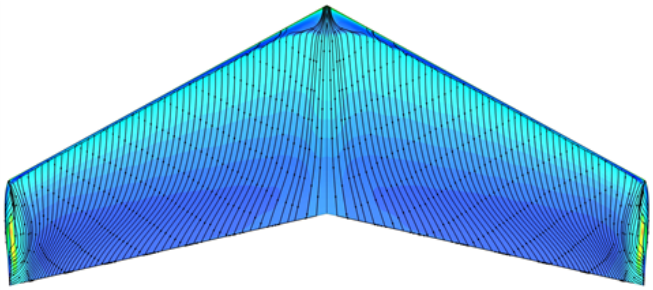

Fig. 8.b. The stream lines and the movement of the fluid flow near the extrados for an AOA value of 13 deg. for a velocity of 50 km/h

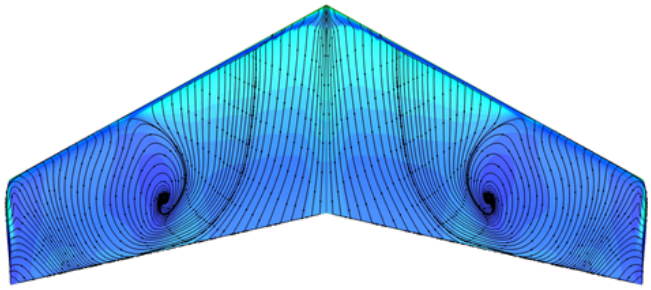

Fig. 8.c.The stream lines and the movement of the fluid flow near the extrados for an AOA value of 14 deg. for a velocity of 50 km/h

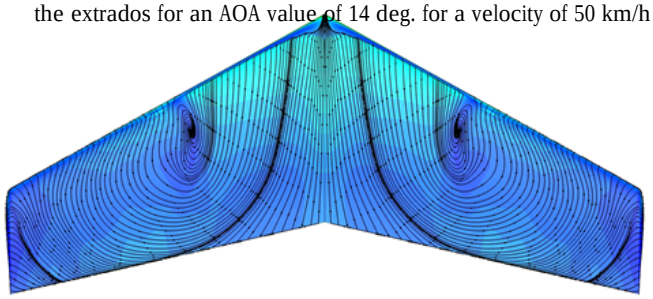

Fig. 8.d. The stream lines and the movement of the fluid flow near the extrados for an AOA value of 15 deg. for a velocity of 50 km/h

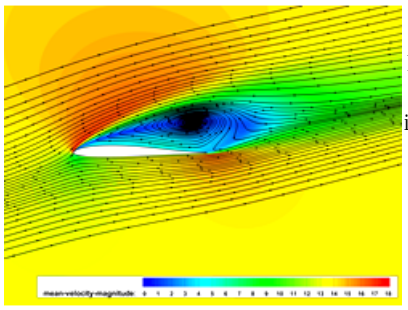

Fig. 9. The phenomenon of detachment could be identified that starts from the leading edge of the wing

Conclusions

This work presents our preliminary research results in order to succeed in building a reliable UAV for environmental purpose [3, 4]. Our aim was to reach a fixed wing flying device with a minimum payload of about 1000 grams and with a flight time over 1 hour. These conditions were minimal and could offer the opportunity to use our partner's research portable devices for environmental investigation.

The most important result is due by the evaluation of the propelling force minimum value and the flight speed. After the computations, the engine should be able to provide at least 3.4 N propelling force, and that only for simple wing without fuselage or other additional sources of resistance.

In the same time, it could be made estimation for the flight speed. Considering our computations and the flight coefficient analysis, the evolution speed should be increased to at least 65 km/h in order to conduct the flight in good condition at a payload capacity of 1.5 kg. This could offer the opportunity to transport the BIRA portable DOAS instruments. In this case, the thrust should be at least 5.5 N.

This work will be further accomplished with the experimental data sets in order to compare these theoretical results.

References

1.BRADLEY, T. H., MOFFITT, B. A., FULLER, T. F., MAVRIS, D. N., AND PAREKH, D. E., Comparison of Design Methods for Fuel-Cell - Powered Unmanned Aerial Vehicles, Journal of Aircraft, Vol. 46, No. 6, 2009, pp. 1945 –1956

2.STONE, R. H., Aerodynamic Modeling of the Wing -Propeller Interaction for a Tail-Sitter Unmanned Air Vehicle, Journal of Aircraft, Vol. 45, No. 1, 2008, pp.198-209.

3.G. TUNA, B. NEFZI, G. CONTE, Unmanned aerial vehicle-aided communications system for disaster recovery, J. Network. Computer App., vol. 41, pp. 27-36, May 2014.

4.F. R. MENTER, M. KUNTZ, R. LANGTRY, Heat and Mass Transfer 4, pp. 625 -632 (2003).

5.JOHN D. ANDERSON Jr., Fundamentals of aerodynamics, Published January by McGraw-Hill Science/Engineering/Math (2001)

6.C.J. BAKER, Journal of Fluids and Structures, Vol. 5, Issue 1, Pages 69-90 (1991)

7.J. J. BERTIN, M.L. SMITH, Aerodynamics for engineers, (1989)

Manuscript received: 19.09.2018